Design, Modeling and Testing of a Flagellum-inspired Soft Underwater Propeller Exploiting Passive Elasticity

Design, Modeling and Testing of a Flagellum-inspired Soft Underwater Propeller Exploiting Passive Elasticity

Marcello Calisti[2], Francesco Giorgio-Serchi[3], Cesare Stefanini[1,2], Madiha Farman[1], Irfan Hussain[1], Costanza Armanini[1], Dongming Gan[1], Lakmal Seneviratne[1], Federico Renda*[1],

***Abstract*— Flagellated micro-organism are regarded as excellent swimmers within their size scales. This, along with the simplicity of their actuation and the richness of their dynamics makes them a valuable source of inspiration to desing continuum, self-propelled underwater robots. Here we introduce a soft, flagellum-inspired system which exploits the compliance of its own body to passively attain a range of geometrical configurations from the interaction with the surrounding fluid. The spontaneous formation of stable helical waves along the length of the flagellum is responsible for the generation of positive net thrust. We investigate the relationship between actuation frequency and material elasticty in determining the steady-state configuration of the system and its thrust output. This is ultimately used to perform a parameter identification procedure of an elastodynamic model aimed at investigating the scaling laws in the propulsion of flagellated robots.**

I. INTRODUCTION

In recent times soft robotics has received growing popularity within the robotics community. This has been spearheaded, in part, by the prospect of tackling challanges which are hardly dealt with by traditial robotics technologies [1], [2], [3], [4]. The ease with which soft robotics prototypes can be manufactured and tested and the fascination for their rich dynamics [5], [6] have also aided in fostering this niche of research. Among the numerous themes in which soft technologies have quickly branched, underwater robotics stands out [7], [8], on one hand, for its added complexity [9], [10] and, on the other hand, for offering an especially suitable context where to test these new kind of machines [11], [12]. Indeed, the close correspondence between the density of the aquatic medium and that of common rubber-like materials of which most soft robots are made of enables underwater soft systems to operate unconstrained by the need for a supportive rigid structure, as it occurs in terrestrial environments [13]. This has positive implications on the broadness of the design space, which has stimulated the development of a vast number of soft bioinspired underwater robots [14], [15], [16], [17].

Within the context of aquatic organisms, major sources of inspiration have been drawn from fish and cephalopods [18], [8], [19], [20], [21], [22] but equally compelling for the purpose of designing bioinspired aquatic vehicles is the study of flagellated bacteria [23] (Fig. 1). These prokaryotic microorganisms sport a vast repertoire of swimming strategies mediated by subtle differences in the structure and kinematics of the flagellum which ultimately enable efficient propulsion at the low Reynolds number scales [24], [25], [26]. A limited range of flagellum-inspired prototypes exist characterized by a stiff structure and ranging in size in the micrometre scale [27] . However, flagella are an interesting case study in soft robotics because they closely resemble, from a morphological and dynamics perspective, some of the archetypal continuum manipulators [28]. Their evolutionary success as low Reynolds number propulsors makes them an appealing source of inspiration for the design of macro-scale mechatronics systems capable of navigating in high-viscosity fuids (e.g. heavy oils) or, alternatively, micro-scale systems suited for locomotion in low-viscosity fluids. Of special interest is the chance to exploit passive structural response and the ensuing kinematics of a flagellum-like body to attend to the transitional regime between the low and intermediate Reynolds numbers. This unique feature, coupled with the capability of performing basic manipulation and the inherent compliance to interaction could make of such flagellum-inspired systems a class of soft robots especially suited for intervention and inspection in fluid-filled conduits of diverse size and fluid composition.

Here we present the first design, model and testing of a macro-scale aquatic soft robot inspired by flagellated prokaryotic bacteria.

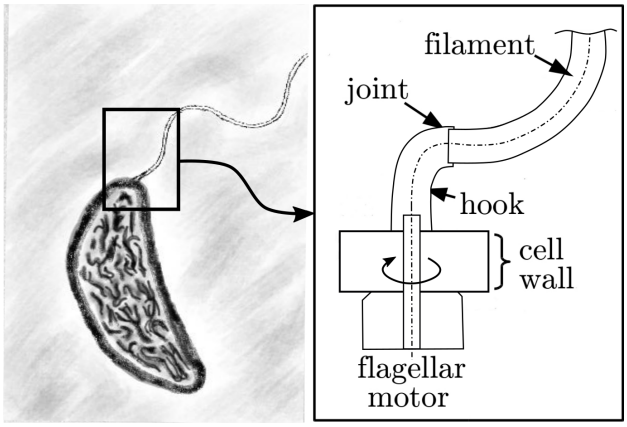

Fig. 1. A *Caulobacter crescentus* and the schematic of the flagellum structure, modified from [29] and [30].

* Corresponding author federico.renda@ku.ac.ae
[1] Khalifa University Center for Autonomous Robotic Systems (KU-CARS), Khalifa University of Science and Technology, Abu Dhabi, UAE.
[2] The BioRobotics Institute, Scuola Superiore Sant'Anna, Pisa, Italy.
[3] Institute of Integrated Micro and Nano Systems of the University of Edinburgh, Edinburgh, UK.

II. FLAGELLUM DESIGN AND FABRICATION

The design of the soft robot is based on the morphology and structure of the flagellum encountered in prokaryotic monotrichous bacteria [31]. This type of bacteria has a single helical flagellum extending from one end of the cell body (Fig. 1). The flagellum of this kind of bacteria is divided in a more flexible end, the filament, and a stiffer base, the hook, which joins the falgellum with the underlying cellular body. The hook is then anchored to a spinning structure, the *flagellar motor*, which is able to rotate in two directions. The torque of this motor is then transmitted across the hook to the filament, whose elastic response in interacting with the surrounding fluid enables the onset of helical waves [32]. The flagella of micro-organisms are commonly referred to as either left-handed or right-handed, identifying with this terminology the tendency of the helical wave to travel from the base to end of the filament or otherwise according to the orientation of the motor rotation [31]. The resulting effect is to either propel the organism forward or backward.

A. Bioinspiration

The choice to mimic prokaryotik flagella is motivated by the chance to exploit the differential mechanical properties of the hook [33] and the filament [34] and the simplicity of its purely rotational actuation [35]. The hook is resistent to torsional stress and stiffer to bending than the flagellum. This arrangement, coupled with a single DOF rotary actuation of the base of the hook caters for a broader range of resultant kinematics than it would in the absence of the hook [36].

Computational studies based on the coupled elastohydrodynamics of the flagella have shown that the driving parameter in the propulsion of these organisms are the rotational frequency of the motor, the stiffness of the hook and the geometrical characteristics of the cellular body [31]. These imply that the swimming speed and efficiency are characterized by two main parameters: the ratio between filament and cell-body length, and the number of helical waves occuring along the length of the filament. The latter of this parameters spontaneously emerges as a response of the geometrical and material properties of the flagellum, the viscosity of the fluid and the actuation of the motor. This is why a comprehensive characterization of the propulsion of flagellated systems must account for the structural response of the passive elastic components, rather than prescribing their pre-determined shape (i.e. a fixed number of helical waves of the filament) [27], [31].

B. Design and Fabrication

Based on the above specifications, the flagellated soft system consists of three components: a soft cone-shaped unit, the *filament*; a pre-curved, torsion-resistant, constant cross-section unit, the *hook* and a rigid cylindrical canister which hosts electronics and a single electric motor which drives the rotation of the hook around its axis of symmetry, Fig. 2 and Fig. 3.

The filament is achieved by casting silicone in a custom-design teflon mould (Fig. 2)(a). This is a cone of basal

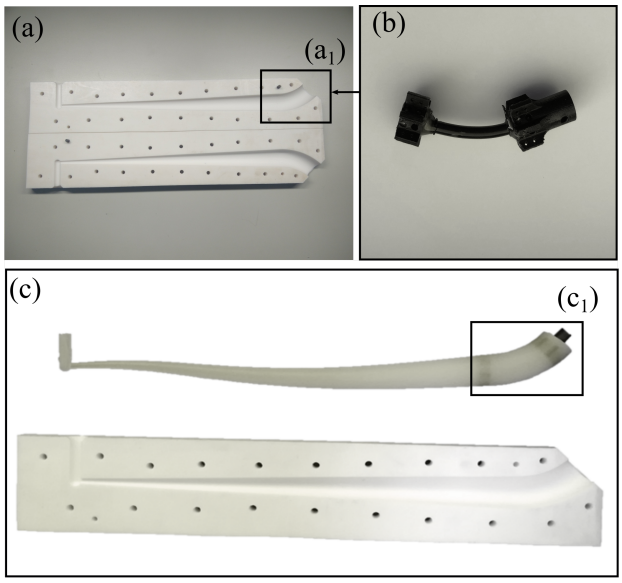

Fig. 2. Components of the flagellated prototype: (a) teflon mould with (a_1) location of the backbone of the hook, (b) the backbone of the hook, (c) silicone cast and (c_1) location of the embedded backbone.

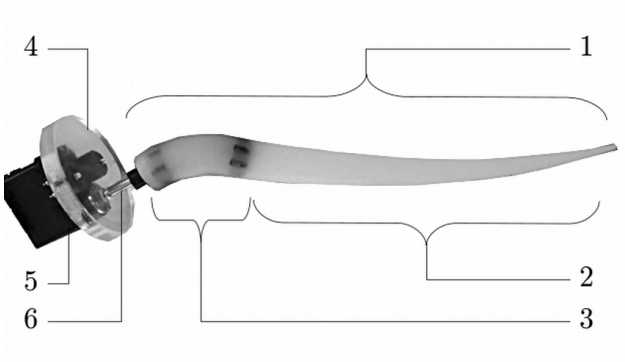

Fig. 3. Flagellum prototype withoud canister: (1) the whole flagellated silicone body, (2) the filament, (3) the hook, with the internal supportive structure visible across the silicone layer, (4) the cover of the canister, (5) the motor and (6) the shaft of the motor linked to the base of the hook.

diameter 25 mm, tip diameter 3 mm and length 300 mm. The hook capability to withstand torsional strain is enabled by a pre-curved backbone, 50 mm long, consisting of a steel coil coated by a polymeric film, depicted in Fig. 2(b). The hook is then connected to the shaft of a Dynamixel AX12 motor Fig. 3, lodged inside a cylindrical waterproof canister 70 mm in diameter and 70 mm long. Waterproofing between the hook and the shaft of the motor is ensured by rubber O-rings. The final prototype is depicted in Fig. 3.

III. DYNAMICS MODELING

To model the elastodynamics of such hybrid soft-rigid locomotor, we employ the geometric and unifying approach developed in [37] and [38], which is a generalization to soft and hybrid systems of the geometric theory of rigid robots due to Brockett [39]. The interested reader is referred to [37], [38] for further details.

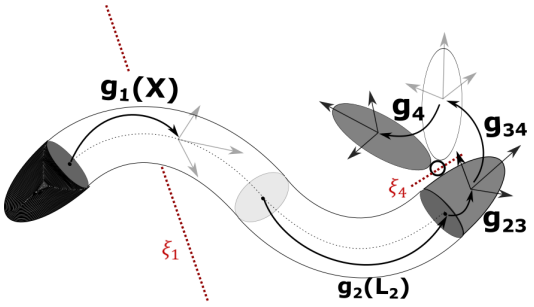

Fig. 4. Schematics of the kinematics of a soft-rigid multi-body system.

According to this formulation, the configuration space of a soft-rigid locomotor is characterized by the traditional generalized variables for the rigid components and a subspace of the six dimensional strain space for the soft ones, where the strains are considered to be section-wise constant for the sake of discretization. Following this definition, the kinematics of a hybrid system can be described by the following equations (Fig. 4):

$$\begin{aligned} \boldsymbol{\xi}_j &= \boldsymbol{B}_j \boldsymbol{q}_j + \bar{\boldsymbol{\xi}}_j \,, \\ \boldsymbol{g}_j(X) &= e^{X\tilde{\boldsymbol{\xi}}_j} \,, \\ \boldsymbol{\eta}_j(X) &= \mathrm{Ad}^{-1}_{\boldsymbol{g}_{ij}\boldsymbol{g}_j(X)} \boldsymbol{\eta}_i + \mathrm{Ad}^{-1}_{\boldsymbol{g}_j(X)} \mathrm{T}_{\boldsymbol{g}_j}(X) \boldsymbol{B}_j \dot{\boldsymbol{q}}_j \,, \end{aligned} \tag{1}$$

where $i < j$ are body (or section) indexes, $\boldsymbol{q}_j \in \mathbb{R}^{n_j}$ is the body j generalized coordinate, $\boldsymbol{B}_j \in \mathbb{R}^{6\times n_j}$ defines the basis for the subspace of motion allowed by the joint (or strain) j, $\boldsymbol{\xi}_j \in \mathbb{R}^6$ is the joint twist, $\bar{\boldsymbol{\xi}}_j \in \mathbb{R}^6$ is a fixed twist modeling the inextensibility constrain (equal to zero for rigid bodies or extensible soft bodies), $X \in [0\, L]$ is the soft body curvilinear abscissa (equal to 1 for the rigid bodies), $\boldsymbol{g}_{ij}\boldsymbol{g}_j \in SE(3)$ represents the j^{th} body position and orientation with respect to the i^{th} body and $\boldsymbol{\eta}_j \in \mathbb{R}^6$ is the body j velocity twist. Finally, $\mathrm{Ad}_{\boldsymbol{g}_j}$ and $\mathrm{T}_{\boldsymbol{g}_j} \in \mathbb{R}^{6\times 6}$ are respectively the Adjoint and Tangent operator of the exponential map [37].

Successive applications of the equations in (1) for all the bodies of the hybrid system, yields to the definition of the geometric Jacobian $\boldsymbol{J}_j \in \mathbb{R}^{6\times n}$ for each soft/rigid body, which relates the generalized coordinate vector $\boldsymbol{q} \in \mathbb{R}^n$ and the j^{th} body velocity twist $\boldsymbol{\eta}_j$ as shown below [37].

$$\boldsymbol{\eta}_j(X) = \boldsymbol{J}_j(X)\dot{\boldsymbol{q}} \,. \tag{2}$$

The knowledge of the geometric Jacobians $\boldsymbol{J}_j$ gives way to the application of standard differential calculus methods, yielding to the dynamic equation of a hybrid system in the standard form [38]:

$$\boldsymbol{M}(\boldsymbol{q})\ddot{\boldsymbol{q}} + \boldsymbol{C}(\boldsymbol{q},\dot{\boldsymbol{q}})\dot{\boldsymbol{q}} + \boldsymbol{K}(\boldsymbol{q}-\boldsymbol{q}^*) = \boldsymbol{\tau} + \boldsymbol{F}(\boldsymbol{q},\dot{\boldsymbol{q}}) \,, \tag{3}$$

where $\boldsymbol{M} \in \mathbb{R}^{n\times n}$ is the generalized mas matrix, $\boldsymbol{C} \in \mathbb{R}^{n\times n}$ is the generalized Coriolis matrix, $\boldsymbol{K} \in \mathbb{R}^{n\times n}$ is the generalized stiffness matrix, $\boldsymbol{q}^* \in \mathbb{R}^n$ is the elastic joint (or strain) reference configuration and $\boldsymbol{\tau} \in \mathbb{R}^n$ is the vector of internal actuation [38]. The generalized external force vector $\boldsymbol{F} \in \mathbb{R}^n$ includes the action of gravity and the fluid-structure interaction. Specifically for our application, the thrust is generated by the dynamic interaction between the soft filament and the surrounding fluid, which, in our model, this is modeled thanks to the Lighthill three-dimensional large amplitude elongated body theory [40], i.e. by a distributed force along the flagellum that reads [37]:

$$\bar{\boldsymbol{F}}_D(X) = -\boldsymbol{D}(X)||\boldsymbol{v}(X)||\boldsymbol{\eta}(X) \,. \tag{4}$$

Above, $\boldsymbol{v}(X) \in \mathbb{R}^3$ is the translational part of the velocity twist $\boldsymbol{\eta}(X)$ and $\boldsymbol{D}(X) \in \mathbb{R}^{6\times 6}$ is the screw matrix of the drag coefficients equal to [37]:

$$\boldsymbol{D}(X) = diag(0,0,0,1/2\pi C_{Dt}, C_{Dn}, C_{Dn}) R(X) \rho_w \,, \tag{5}$$

where $R(X) \in \mathbb{R}$ is the radius of the flagellum at X, C_{Dt} and C_{Dn} are respectively the tangential and normal drag coefficients, and ρ_w is the water density.

To model the three parts of our artificial flagellum we have employed two different kinds of soft bodies and one rigid body. The *flagellar motor* is simply modeled as an actuated revolute joint, the *hook* is represented by an inextensible Cosserat rod with constant curvatures and constrained torsion, while the *filament* is described by an inextensible Kierchhoff-Love rod. Accordingly, the motion subspaces are defined by the following basis and inextensibility constrain twists (assuming the x-axis lying along the rotation axis for the revolute joint and along the midline tangent for the rods):

$$\boldsymbol{B}_m = \begin{bmatrix} 1 \\ 0 \\ 0 \\ 0 \\ 0 \\ 0 \end{bmatrix}, \boldsymbol{B}_h = \begin{bmatrix} 0 & 0 \\ 1 & 0 \\ 0 & 1 \\ 0 & 0 \\ 0 & 0 \\ 0 & 0 \end{bmatrix}, \boldsymbol{B}_f = \begin{bmatrix} 1 & 0 & 0 \\ 0 & 1 & 0 \\ 0 & 0 & 1 \\ 0 & 0 & 0 \\ 0 & 0 & 0 \\ 0 & 0 & 0 \end{bmatrix}, \bar{\boldsymbol{\xi}}_h = \bar{\boldsymbol{\xi}}_f = \begin{bmatrix} 0 \\ 0 \\ 0 \\ 1 \\ 0 \\ 0 \end{bmatrix}. \tag{6}$$

For what concerns the net motion of the canister, we employ two different models in this work according to the phenomena we want to describe. In section III-A, a constrained rectilinear motion is used to select the appropriate number of sections into which divide the filament, while in the experimental section IV, a controlled free motion is tested in order to measure the flagellum dynamic reaction with the surrounding fluid (including thrust). Thus, the net motion subspaces are defined by the following basis twists respectively (assuming the x-axis is aligned with the heading):

$$\boldsymbol{B}_c = \begin{bmatrix} 0 \\ 0 \\ 0 \\ 1 \\ 0 \\ 0 \end{bmatrix}, \boldsymbol{B}_c = \begin{bmatrix} 1 & 0 & 0 & 0 & 0 & 0 \\ 0 & 1 & 0 & 0 & 0 & 0 \\ 0 & 0 & 1 & 0 & 0 & 0 \\ 0 & 0 & 0 & 1 & 0 & 0 \\ 0 & 0 & 0 & 0 & 1 & 0 \\ 0 & 0 & 0 & 0 & 0 & 1 \end{bmatrix}. \tag{7}$$

In both cases, the rotation of the motor $q_m(t) \in \mathbb{R}$ is prescribed, leading to two mixed forward-inverse dynamic problems. For the constrained rectilinear swimming, the unknowns are the time functions of the generalized coordinates $q_c(t) \in \mathbb{R}$, $\boldsymbol{q}_h(t) \in \mathbb{R}^2$, $\boldsymbol{q}_f(t) \in \mathbb{R}^3$ and the torque exterted by the motor $\tau_m(t) \in \mathbb{R}$ to guarantee the required shaft rotation.

For the controlled free motion, the net discplacement of the canister is also prescribed, leaving as unknowns the reaction forces/torques $\boldsymbol{\tau}_c(t) \in \mathbb{R}^6$ exerted by the ground to keep the canister stationary, the torque exterted by the motor $\tau_m(t)$ and the motion of the rest of the bodies $\boldsymbol{q}_h(t)$, $\boldsymbol{q}_f(t)$. Both mixed problems can be solved by inverting and numerically integrating a proper recombination of the columns of (3) ([41], example 9.1). Alternatively, the recursive algorithm described in [37], [38] can be employed.

A. Coarseness Selection

The accuracy in capturing the elastodynamic response of the system based on actuation is dependent on the capability of the model to describe the variable cross-section of the flagellum. This is accounted for by representing the flagellum with a finite series of constant cross-section segments arranged along the length of the flagellum according to a gradient of decreasing girth.

Numerical accuracy is postulated on the capability of the model to capture a reference parameter (e.g. swimming speed) at varying degree of resolution, similarly to the process of grid independence analysis of other mesh-based solvers. The resolution is determined, here, by the number of descrete constant cross-section segments employed to model the flagellum. By taking as a reference a constrained linear motion of the apparatus, we computed the forward speed of the body obtained at steady state with respect to the angular speed of the shaft of the motor. Repeating this test with increasing number of segments, we look for convergence of the control parameter (i.e. swimming speed).

As shown in Fig.5, we found that the model were generating non-physical behavior for a 2-sections filament at high rotational speed, while no significant differences where observed for the 3-, 4-, and 5-sections case. If the 5-section case is taken as the reference value, the 3 and 4 segment output show a convergence mean error of 4.5 and 4.3 % respectively. Thus, we selected the 3-sections model for the rest of the simulations in this work.

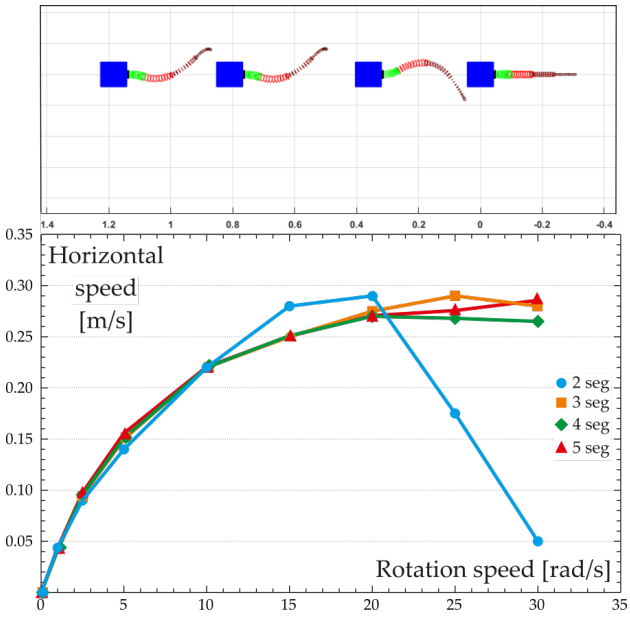

Fig. 5. Output from the numerical results of the elastodynamic model. Top figure: helical wave formation during motor rotation (5 rad/s) at four subsequent timeframes $t = 0$, 4.5, 7.5 and 10 sec. Bottom figure: convergence of discretization accuracy based on number of segments.

IV. EXPERIMENTAL TESTING

The characterization of the propulsive routine of the flagellated soft robot requires to correlate the helical wave formation along the filament with the magnitude of the net forward thrust. To do so, it is necessary to capture the kinematic of the elastic filament as a response to both the motor rotation and the interaction with the surrounding fluid. While a full characterization of this dynamic response requires the prototype to be observed in a towed-test case or in a self-propelled case, the first set of tests described here will be performed in a controlled environment, with the prototype held stationary. These tests will serve the purpose of validating the dynamics model as well as characterizing a start-from-rest manoeuver.

A. Set-up

The experimental setup consists of a fixed stationary support unit onto which the prototype of Section II-B is anchored via an ATI mini 6DOF force/torque sensor. The rig support is suspended over a water tank 500 mm long and 500 mm wide filled with fresh water to a depth of 370 mm. The flagellum prototype is immersed in water and allowed to rest vertically, as depicted in Fig. 6, and linked to the force sensor via the motor canister. Any displacement of the flagellum as a result of the motor rotation is transferred to the sensor which records linear force along the x, y and z directions and torque around these axis. The ATI sensor samples at a frequency of 1000Hz at a resolution of 1/50 N and 1/4000 Nm respectively for the linear force and torque.

Two cameras in stereo configuration are placed outside the water tank. Commercial SONY DC-W800 color cameras were used, with a spatial resolution of 20.1 MP, and temporal resolution of 30 fps. A total of six passive markers are placed along the prototype, two within the hook, and four along the filament. A Direct Linear Transformation algorithm [42], previously employed for soft robots reconstruction [43] in water environment, was used to obtain the position in space of the markers. Eight positions within the tank were used as calibration points.

In order to characterize the propulsive response due to flagellum actuation and adaptive response, three parameters need to be characterzied simultaneously: the motor rotational speed, the emerging helical wave patter of the filament and the resulting thrust (i.e. linear force along the z axis). To do so, three silicone hardness and three rotational frequencies are tested, running each trial for 35.0s in order to ascertain quasi-steady-state attainment and performing three repetition of each trial. The three silicone hardness tested are the Smooth-On™ Ecoflex™ 0050, Dragon Skin™ FX-Pro and Dragon Skin™ 30, whose parameters are reported in TableI.

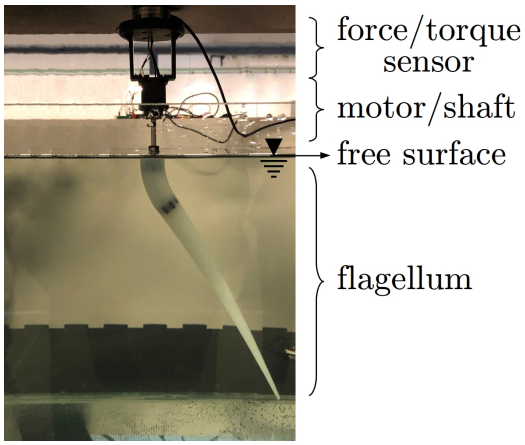

Fig. 6. Experimental set-up of the static thrust characterization of the flagellated prototype.

TABLE I
SILICONE PARAMETERS

	100% Modulus E [Pa]	Density ρ [kg/m^3]
Ecoflex™ 0050	82737	1070
Dragon Skin™ FX-Pro	260622	1062
Dragon Skin™ 30	592949	1080

B. Free parameters estimation

The only unknown parameters in the model setup are the sectionwise tangential and normal drag coefficients C_{Dt} and C_{Dn}, see eq. (5). During flagellum rotation, each section of the filament undergoes extensive deformation and is exposed to the incoming flow with a finite angle of attack. Therefore these coefficients cannot be simply inferred from geometric arguments (i.e. using a strip-based approximation where the drag coefficient of a circular cylinder is used). Instead we choose to identify these coefficients, effectively treating them as a proxy for the flagellum steady-state three dimensional shape. By associating varying drag coefficients with varying rotational speed of the body, we are essentially inferring the dependency of these coefficients on the length-averaged angle-of-attack of the flagellum with the incoming flow. To do so, we used a constrained optimization with the Nelder–Mead method and estimate C_{Dt} and C_{Dn} from the tridimensional shape of the rotating prototype. The problem was formulated as a minimum optimization of the function $e(X) = ||\boldsymbol{T} - \boldsymbol{m}(\boldsymbol{x})||$, where $\boldsymbol{T}$ is the target vector of the marker positions (extracted with the aid of the vision system) of the flagellum at steady state, $\boldsymbol{x}$ is the variables' vector $\boldsymbol{x} = (C_{Dn}, C_{Dt})$, where each element is constrained between [0.001 25], and $\boldsymbol{m}$ is the model.

V. RESULTS AND DISCUSSION

The experimental trials were performed for 35 seconds each, and the flagellum reached steady state configuration after a few seconds of rotation. While at steady state rotation, the markers moved along circular-shaped paths parallel to the ground which, when tracked, give rise to the threeedimensional projection shown in Fig. 8. Data were interpolated

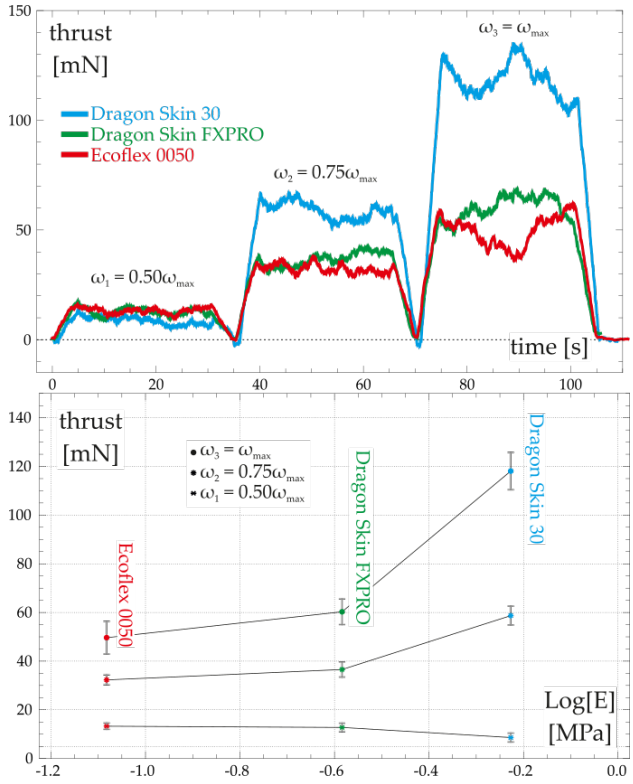

Fig. 7. Vertical thrust generated by three silicone prototype with different elasticity at various angular velocity of the shaft. ω_{max} is the highest angular velocity provided by the motor, equal to 5.1 [rad/s].

to minimize the mean square error with the ideal circular shapes.

A. Thrust analysis

Thrust measurement highlighted a clear relationship between flagellum rotational speed and vertical net force, Fig.7a. The experiments showed a good degree of reproducibility with an observable, repeatable pattern where the force signal would undergo an initial short transient eventually settling onto a constant, quasi-steady value. Larger oscillations of the thrust signal were observed at higher rotational speeds. Thrust dependency to material stiffness was also observed, as demonstrated in Fig.7(b). Interestingly, thrust measurement shows a divergent trend where stiffer flagella produced the highest force at higher speeds, while softer flagella produced higher thrust at lower speeds. However, it is worth to notice that a rigid flagellum equipped with the planar reference shape adopted here would not lead to the formation of the thrust-provoking helical wave. This encourages further exploration of a wider range of flagellum stiffness and rotational speeds to fully characterize the thrust generation of this novel propulsion mechanism.

B. Dynamic model parameter identification

The comparison between experimental and simulated radii of the circumferences showed average errors lower than 2.5mm, 0.7% of the total length. As expected, the error increased from the base to the tip, where a difference of

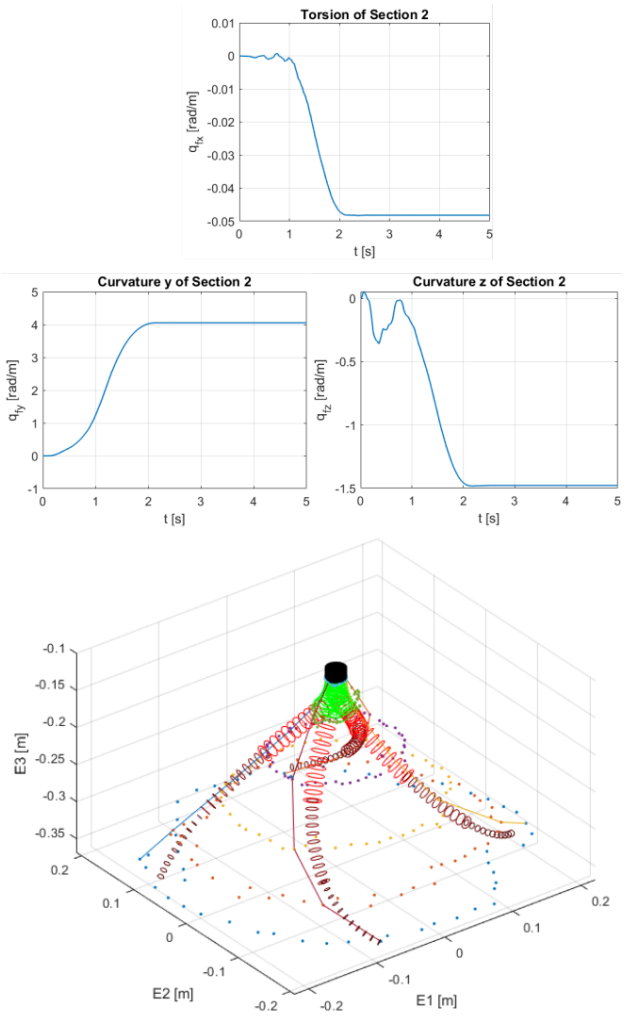

Fig. 8. Reconstructed (solid lines and dots) and simulated flagellum made of Dragon Skin™ 30 while steadily rotating at 3.825 [rad/s].

around 5mm (1.4%) was observed, while the error at the base of the hook was lower than 1mm (0.3%). An overview of the comparison between reconstructed and simulated shape is given in Fig. 8, together with the typical deformations involved (middle section of the filament). Within the context of soft manipulators, our errors stands closer to the accuracy obtained by [37], [28]. Discrepancies between recorded and modelled shape configuration are attributed to the kinematic approximation (6), the linear elasticity assumption and the simplicity of the hydrodynamic model (4), which neglects the inertial and viscous fluid effects arising from the proximity of the tank end walls. Nevertheless, the good agreement between the reconstructed features and the thrust elect our model as a useful tool to estimate the performance of the robot and guide the design optimization.

The identification of constant drag coefficients for all X and for each test, reported in II, results in a very good matching between the predicted and experimental thrust, as shown in Tab. III.

The present attempt represents a good starting point for future improvements of the thrust generation model for such

TABLE II

IDENTIFIED TANGENTIAL C_{Dt} AND NORMAL C_{Dn} DRAG COEFFICIENTS

		ω [rad/s]		
		2.55	3.825	5.1
Dragon Skin™ 30	C_{Dt} [-]	0.19	0.001	0.001
	C_{Dn} [-]	0.72	0.85	0.96
Dragon Skin™ FX-Pro	C_{Dt} [-]	0.19	0.19	0.19
	C_{Dn} [-]	0.79	0.85	0.85
Ecoflex™ 0050	C_{Dt} [-]	0.17	0.16	0.18
	C_{Dn} [-]	0.95	0.85	0.85

TABLE III

AVERAGE EXPERIMENTAL THRUST T_e, OBTAINED FROM SIMULATIONS T_s, AND RELATIVE ERROR FOR DIFFERENT SPEEDS ω

		ω [rad/s]		
		2.55	3.825	5.1
Dragon Skin™ 30	T_e [mN]	8.61	58.71	118.09
	T_s [mN]	8.69	58.03	117.42
	Err [%]	0.9	1.2	0.6
Dragon Skin™ FX-Pro	T_e [mN]	12.76	36.56	60.28
	T_s [mN]	13	36.73	59.5
	Err [%]	1.9	0.4	1.3
Ecoflex™ 0050	T_e [mN]	13.27	32.30	49.65
	T_s [mN]	13.5	31.9	49.67
	Err [%]	1.7	1.2	0.04

unexplored propulsion mechanism. In fact, the proposed framework allows to include lift coefficients in the off-diagonal terms of (5) as well as to compute the formal integration of varying drag and lift coefficients along the filament length.

VI. CONCLUSIONS AND FUTURE WORKS

In this work we presented a methodology for the design and development of a novel generation of underwater propulsors which draw their inspiration from flagellated organisms. The conceptual design of the propeller is inspired from a unique biological model, which features a two-part flagellum (namely *hook* and *filament*) with different mechanical, geometrical and functional characteristics. The whole rotating flagellum is accurately modeled as a continuum, deformable structure, both in fixed-body and linear motion conditions, and was eventually employed in a parameter identification process which aims at identifying the salient features in thrust generation of such unconventional systems.

From our results, we confirmed the agreement between our model and the behavior of the prototype, with an accuracy in reconstruction which matched other state-of-the-art continuum models. The applicability of such solution as novel propulsion methodology couches into the thrust obtained from the experiments, which possibly allow us to optimize shape, material and actuation speed to improve the performance of the device.

The work presented in this manuscript provides the basis to understand the leading terms and their interplay in the propulsion of these kind of hyperelastic systems and generalize the results achieved in this way to a broader family of flagellated, soft robots.

ACKNOWLEDGMENT

This research was supported by Dr. Renda' Faculty Start-up Fund FSU-2018-08, Khalifa University of Science and Technology.

REFERENCES

[1] R. Woodman, A. Winfield, C. Harper, and M. Fraser, "Building safer robots: Safety driven control," *The International Journal of Robotics Research*, 2012.

[2] A. Mortl, M. Lawitzky, A. Kucukyilmaz, M. Sezgin, C. Basdogan, and S. Hirche, "The role of roles: Physical cooperation between humans and robots," *The International Journal of Robotics Research*, 2012.

[3] K. C. Galloway, K. P. Becker, B. Phillips, J. Kirby, S. Licht, D. Tchernov, R. J. Wood, and D. F. Gruber, "Soft robotic grippers for biological sampling on deep reefs," *Soft Robotics*, vol. ahead of print, 2016.

[4] L. Ascari, C. Stefanini, U. Bertocchi, and P. Dario, "Robot-assisted endoscopic exploration of the spinal cord," *Proceedings of the Institution of Mechanical Engineers, Part C: Journal of Mechanical Engineering Science*, vol. 224, no. 7, pp. 1515–1529, 2010. [Online]. Available: https://doi.org/10.1243/09544062JMES2017

[5] G. Chirikjian, "A continuum approach to hyper-redundant manipulator dynamics," in *Intelligent Robots and Systems '93, IROS '93. Proceedings of the 1993 IEEE/RSJ International Conference on*, vol. 2, Jul 1993, pp. 1059–1066.

[6] R. J. Webster and B. A. Jones, "Design and kinematic modeling of constant curvature continuum robots: A review," *The International Journal of Robotics Research*, vol. 29, no. 13, pp. 1661–1683, 2010.

[7] A. D. Marchese and D. Rus, "Design, kinematics, and control of a soft spatial fluidic elastomer manipulator," *The International Journal of Robotics Research*, 2015.

[8] M. Calisti, G. Picardi, and C. Laschi, "Fundamentals of soft robot locomotion," *Journal of The Royal Society Interface*, vol. 14, no. 130, 2017.

[9] M. J. Lighthill, "Aquatic animal propulsion of high hydromechanical efficiency," *Journal of Fluid Mechanics*, vol. 44, pp. 265–301, 11 1970.

[10] F. Candelier, F. Boyer, and A. Leroyer, "Three-dimensional extension of lighthill's large-amplitude elongated-body theory of fish locomotion," *Journal of Fluid Mechanics*, vol. 674, pp. 196–226, 2011.

[11] M. Calisti and C. Laschi, "Morphological and control criteria for self-stable underwater hopping," *Bioinspiration & Biomimetics*, vol. 13, no. 1, p. 016001, nov 2017.

[12] F. Giorgio-Serchi and G. D. Weymouth, "Underwater soft robotics, the benefit of body-shape variations in aquatic propulsion," in *Soft Robotics: Trends, Applications and Challenges*, C. Laschi, J. Rossiter, F. Iida, M. Cianchetti, and L. Margheri, Eds. Cham: Springer International Publishing, 2017, pp. 37–46.

[13] F. Corucci, N. Cheney, F. Giorgio-Serchi, J. Bongard, and C. Laschi, "Evolving soft locomotion in aquatic and terrestrial environments: Effects of material properties and environmental transitions," *Soft Robotics*, vol. 5, no. 4, pp. 475–495, 2018.

[14] J. Abbott, C. M. Lagomarsino, L. Zhang, L. Dong, and B. J. Nelson, "How should microrobots swim?" *The International Journal of Robotics Research*, 2009.

[15] J. Conte, Y. Modarres-Sadeghi, M. N. Watts, F. S. Hover, and M. S. Triantafyllou, "A fast-starting mechanical fish that accelerates at 40 m s 2," *Bioinspiration & Biomimetics*, vol. 5, no. 3, p. 035004, 2010.

[16] M. Sfakiotakis, A. Kazakidi, A. Chatzidaki, T. Evdaimon, and D. Tsakiris, "Multi-arm robotic swimming with octopus-inspired compliant web," in *Intelligent Robots and Systems (IROS 2014), 2014 IEEE/RSJ International Conference on*, Sept 2014, pp. 302–308.

[17] C. Stefanini, G. Orlandi, A. Menciassi, Y. Ravier, G. La Spina, S. Grillner, and P. Dario, "A mechanism for biomimetic actuation in lamprey-like robots," in *The First IEEE/RAS-EMBS International Conference on Biomedical Robotics and Biomechatronics, 2006. BioRob 2006.*, Feb 2006, pp. 579–584.

[18] A. D. Marchese, D. Onal Cagdas, and D. Rus, "Autonomous soft robotic fish capable of escape maneuvers using fluidic elastomer actuators," *Soft Robotics*, vol. 1, no. 1, pp. 75–673, March 2014.

[19] F. Giorgio-Serchi, A. K. Lidtke, and G. D. Weymouth, "A soft aquatic actuator for unsteady peak power amplification," *IEEE/ASME Transactions on Mechatronics*, vol. 23, no. 6, pp. 2968–2973, Dec 2018.

[20] F. Renda, F. Giorgio-Serchi, F. Boyer, C. Laschi, J. Dias, and L. Seneviratne, "A unified multi-soft-body dynamic model for underwater soft robots," *The International Journal of Robotics Research*, vol. 37, no. 6, pp. 648–666, 2018.

[21] C. Stefanini, S. Orofino, L. Manfredi, S. Mintchev, S. Marrazza, T. Assaf, L. Capantini, E. Sinibaldi, S. Grillner, P. Wallén, and P. Dario, "A novel autonomous, bioinspired swimming robot developed by neuroscientists and bioengineers," *Bioinspiration & Biomimetics*, vol. 7, no. 2, p. 025001, may 2012.

[22] L. Manfredi, T. Assaf, S. Mintchev, S. Marrazza, L. Capantini, S. Orofino, L. Ascari, S. Grillner, P. Wallén, Ö. Ekeberg, *et al.*, "A bioinspired autonomous swimming robot as a tool for studying goal-directed locomotion," *Biological cybernetics*, vol. 107, no. 5, pp. 513–527, 2013.

[23] A. Jamel, U. K. Cheang, J. D. Martindale, M. Jabbarzadeh, H. C. Fu, and M. Kim, "Bacteria-inspired nanorobots with flagellar polymorphic transformations and bundling," *Nature Scientific Report*, vol. 7, 2017.

[24] C. Brennen and H. Winet, "Fluid mechanics of propulsion by cilia and flagella," *Annual Review of Fluid Mechanics*, vol. 9, no. 1, pp. 339–398, 1977.

[25] E. M. Purcell, "The efficiency of propulsion by a rotating flagellum," *Proceedings of the National Academy of Sciences*, vol. 94, no. 21, pp. 11 307–11 311, 1997.

[26] E. Lauga and T. Powers, "The hydrodynamics of swimming microorganisms," *Proceedings of the National Academy of Sciences*, vol. 72, no. 096601, 2009.

[27] J. Singleton, E. Diller, T. Andersen, S. Regnier, and M. Sitti, "Micro-scale propulsion using multiple flexible artificial flagella," in *2011 IEEE/RSJ International Conference on Intelligent Robots and Systems*, Sep. 2011, pp. 1687–1692.

[28] F. Renda, M. Giorelli, M. Calisti, M. Cianchetti, and C. Laschi, "Dynamic model of a multibending soft robot arm driven by cables," *Robotics, IEEE Transactions on*, vol. 30, no. 5, pp. 1109–1122, Oct 2014.

[29] J. S. Schuhmacher, G. Bange, and K. M. Thormann, "How bacteria maintain location and number of flagella?" *FEMS Microbiology Reviews*, vol. 39, no. 6, pp. 812–822, 07 2015.

[30] K. Yonekura, S. Maki, D. Morgan, D. DeRosier, F. Vonderviszt, K. Imada, and K. Namba, "The bacterial flagellar cap as the rotary promoter of flagellin self-assembly," *Science*, vol. 290, no. 5499, pp. 2148–2152, 2000.

[31] Y. Park, Y. Kim, and S. Lim, "Locomotion of a single-flagellated bacterium," *Journal of Fluid Mechanics*, vol. 859, p. 586–612, 2019.

[32] L. Koens, H. Zhang, M. Moeller, A. Mourran, and E. Lauga, "The swimming of a deforming helix," *The European Physical Journal E*, vol. 41, no. 10, p. 119, Oct 2018.

[33] F. Samatey, H. Matsunami, K. Imada, S. Nagashima, T. R. Shaikh, D. Thomas, J. Chen, D. DeRosier, A. Kitao, and K. Namba, "Structure of the bacterial flagellar hook and implication for the molecular universal joint mechanism," *Nature*, vol. 431, pp. 1062–1068, 2004.

[34] F. A. Samatey, K. Imada, S. Nagashima, F. Vonderviszt, T. Kumasaka, M. Yamamoto, and K. Namba, "Structure of the bacterial flagellar protofilament and implications for a switch for supercoiling," *Nature*, vol. 410, pp. 331–337, 2001.

[35] D. DeRosier, "The turn of the screw: The bacterial flagellar motor," *Cell*, vol. 93, no. 1, pp. 17–20, 1998.

[36] H. Shum and E. A. Gaffney, "The effects of flagellar hook compliance on motility of monotrichous bacteria: A modeling study," *Physics of Fluids*, vol. 24, no. 6, p. 061901, 2012.

[37] F. Renda, F. Boyer, J. Dias, and L. Seneviratne, "Discrete cosserat approach for multisection soft manipulator dynamics," *IEEE Transactions on Robotics*, vol. 34, no. 6, pp. 1518–1533, Dec 2018.

[38] F. Renda and L. Seneviratne, "A geometric and unified approach for modeling soft-rigid multi-body systems with lumped and distributed degrees of freedom," in *2018 IEEE International Conference on Robotics and Automation (ICRA)*, May 2018, pp. 1567–1574.

[39] R. W. Brockett, "Robotic manipulators and the product of exponentials formula," in *Mathematical Theory of Networks and Systems*. Springer Berlin Heidelberg, 1984, pp. 120–129.

[40] F. Boyer, M. Porez, and A. Leroyer, "Poincaré cosserat equations for the lighthill three-dimensional large amplitude elongated body theory: Application to robotics," *Journal of Nonlinear Science*, vol. 20, no. 1, pp. 47–79, 2010.

[41] R. Featherstone, *Rigid Body Dynamics Algorithms*. Springer New York, 2008.

[42] T. L. Hedrick, "Software techniques for two-and three-dimensional kinematic measurements of biological and biomimetic systems," *Bioinspiration & biomimetics*, vol. 3, no. 3, p. 034001, 2008.

[43] M. Giorelli, F. Renda, M. Calisti, A. Arienti, G. Ferri, and C. Laschi, "Learning the inverse kinetics of an octopus-like manipulator in three-dimensional space," *Bioinspiration & biomimetics*, vol. 10, no. 3, p. 035006, 2015.